Article

Analysis of fast fluorescence kinetics of a single cyanobacterium trapped in an optical microcavity

Tim Rammler [1,2], Frank Wackenhut [1], Johanna Rapp [3], Sven zur Oven-Krockhaus [1,2], Karl Forchhammer [3], Klaus Harter [2,*] and Alfred J. Meixner [1,*]

[1] Institute for Physical & Theoretical Chemistry, University of Tübingen, 72076 Tübingen, Germany
[2] Center for Plant Molecular Biology (ZMBP), University of Tübingen, 72076 Tübingen, Germany
[3] Interfaculty Institute of Microbiology and Infection Medicine, University of Tübingen, 72076 Tübingen, Germany
* Correspondence: klaus.harter@zmbp.uni-tuebingen.de; Tel.: +49-(0)-7071-2972605 and alfred.meixner@uni-tuebingen.de; Tel.: +49-(0)-7071-2976903

Abstract: Photosynthesis is one the most important biological processes on earth, producing life-giving oxygen and is the basis for a large variety of plant products. Measurable properties of photosynthesis provide information about its biophysical state and, in turn, the physiological conditions of a photoautotrophic organism. For instance, chlorophyll fluorescence of an intact photosystem is not linear as in the case of a single fluorescent dye in solution, but shows temporal changes related to the quantum yield of the photosystem. Commercial photosystem analyzers already use the fluorescence kinetics characteristics of photosystems to infer the viability of organisms under investigation. Here, we provide a novel approach based on an optical Fabry-Pérot microcavity or that enables the readout of photosynthetic properties and activity for an individual cyanobacterium. This approach offers a completely new dimension of information, which would normally be lost due to averaging in ensemble measurements obtained from a large population of bacteria.

Keywords: cyanobacteria, photosystem, fast fluorescence kinetics, optical microcavity, fluorescence microscopy

1. Introduction

Photosynthesis by cyanobacteria is one of the most important processes on earth. It was responsible for the oxygenation of the earth about 2.4 billion years ago, which enabled the subsequent development of multicellular life forms [1]. Even today, cyanobacterial photosynthesis significantly contributes to oxygen (O_2) generation during the process of carbon fixation typically from CO_2 [2]. Furthermore, ancient cyanobacteria were the precursor of endosymbiotic chloroplasts [3], which also enable higher plants to produce O_2 and the chemical energy equivalents needed to fix CO_2. Because of the importance of this process, and with the hope of replicating this process as organic solar cells, it is compelling to understand this process in its entirety. Although there is much already known, there are still unexplained phenomena in the photosynthetic process. One example is the energy transfer in photosystem 2 (PS2) from the absorption of a photon in the peripheral pigments to the reaction center, where the energy is used to split water. It is still not conclusively understood why the efficiency of this process is as high as 99% and whether this is related to non-trivial quantum optical effects [4].

The study of photosynthetic organisms by chlorophyll fluorescence kinetics has become an effective method to detect even small changes in the photosynthetic process [5]. Among other techniques, this non-invasive method is already routinely used for the analysis of photosynthetic microorganisms, plant cell cultures and whole plants [6]. In this work, we present a novel method to study the photosynthetic efficiency in a living individual cyanobacterium on the basis of the well-studied Kautsky effect. Here, the kinetic

 doi:10.20944/preprints202211.0199.v1

behavior of the fluorescence emission is used to determine the quantum yield [7]. In contrast to previous analyses performed at the population level, our method enables one to determine the photosynthetic activity of an individual cell, exposing effects that are usually lost due to population averaging.

To enable the very detailed analysis of the Kautsky effect and, thus, the photosynthetic efficiency at the single cell level, living cyanobacteria were placed in an optical Fabry-Pérot microcavity [9]. The microresonator is composed of two semi-transparent mirrors, with a mirror separation of ~2 µm giving rise to microcavity resonances in the visible spectral range. In addition to strong coupling, a microcavity can also increase or decrease the spontaneous emission rate of a chromophore by tuning the resonance of the microcavity to the fluorescence of the chromophore or away from the fluorescence. This effect is called the Purcell effect [11] [12] [36] and shortens the fluorescence lifetime (FLT) of the chromophore for an on-resonant microcavity and prolongs it for an off-resonant microcavity [9]. Due to the small space inside the microcavity, it is difficult or impossible to use near-probe dependent methods, such as O_2 detectors to determine the quantum yield *in vivo*. In order to capture the true photosynthetic efficiency of PS2, the experimental setup was designed as to minimize and eliminate residual phycobilisome (PBS) and photosystem 1 (PS1) fluorescence signals [8]. Our experimental approach offers a completely new way of knowledge about the PS2 activity, which would normally be lost due to averaging in ensemble measurements using a large cyanobacterial population.

2. Results

2.1 Theoretical introduction and technical challenges

In our experiments, we investigated the unicellular cyanobacterium *Synechocccus elongatus* strain PCC 7942 (*S. elongatus*), a widely used model organism for photosynthetic research [13] [14]. We have determined the quantum yield of individual cyanobacteria by analyzing the fast fluorescence kinetics (FFK) of PS2. The principle is based on the Kautsky effect [7] which describes the variable fluorescence (F_V) after dark adaptation as a function of the irradiation time with actinic light (photosynthesis activating light) (see Fig. 1A). The Kautsky effect divides the temporal evolution of the fluorescence signal into two regions: a short, initial time window of the fast fluorescence increase in intensity (fast fluorescence kinetics, FFK) occurring in the microseconds time range (see Fig. 1A/C/D, blue area), and the subsequent region of slow fluorescence kinetics (SFK), which describes the slow decrease occurring in the seconds to minutes time range (see Fig. 1A/C/D, green area). The photosystem of *S. elongatus* was spectrally analyzed to ensure that, according to the Kautsky effect, only the PS2 core antenna chlorophyll fluorescence was measured. The absorption spectrum of *S. elongatus* cells shows four distinct bands: the chlorophyll a soret band at 440 nm [15], the carotenoid band at 500 nm [16], the PBS band at 630 nm [17], and the Q_y band of chlorophyll a at 680 nm [18] (Fig. 1B).

Preprints (www.preprints.org) | NOT PEER-REVIEWED | Posted: 10 November 2022 doi:10.20944/preprints202211.0199.v1

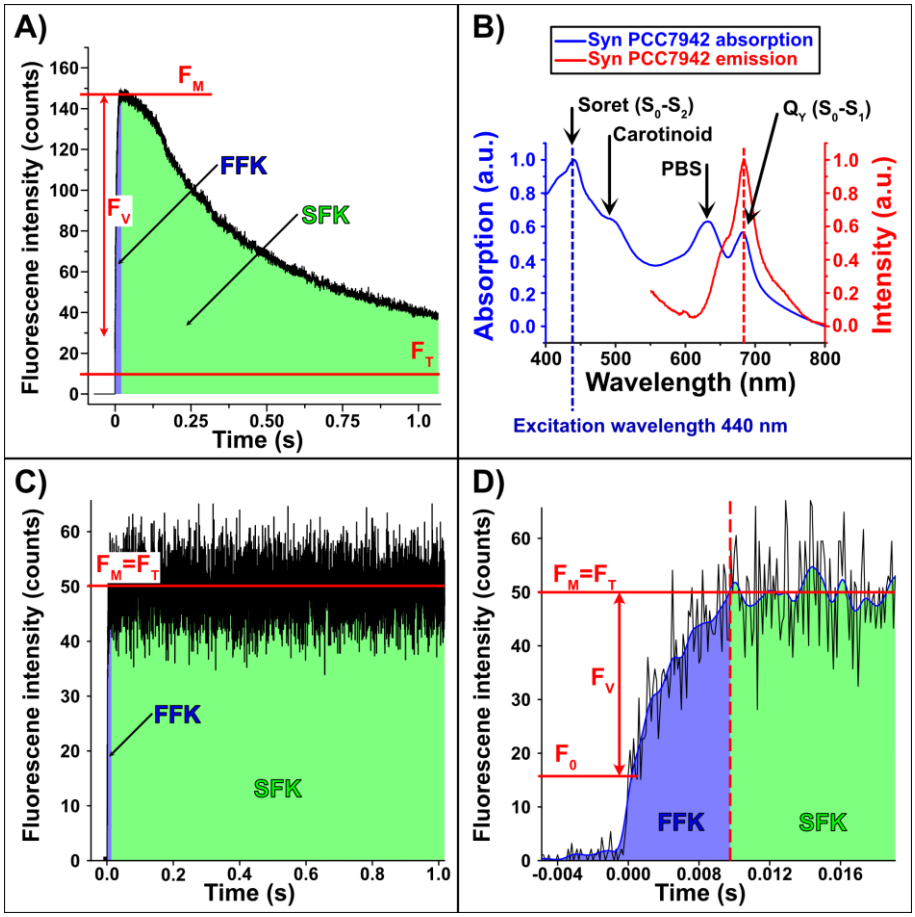

Figure 1. (A) Fluorescence intensity time trace of *S. elongatus* population excited with saturating light intensity. Shown in red: the maximum fluorescence intensity (F_M) and the terminal fluorescence (F_T) intensity according to the Kautsky effect. The blue area indicates the temporal range of the fast fluorescence kinetics (FFK) and the green area the range of the slow fluorescence kinetics (SFK). **(B)** Normalized fluorescence (red) and absorption (blue) spectra of *S. elongatus* measured in BG11 medium [19]. The bacteria were excited with a laser of 440 nm (blue dashed line). The bacteria have both an absorption and emission maximum at approx. 680 nm (black dashed line). **(C)** Fluorescence intensity time trace of *S. elongatus* after treatment with 3-(3,4-Dichlorophenyl)-1,1-dimethylurea (DCMU). By spiking with DCMU, F_T no longer decreases to the same level as seen in (A), because electron transport between PS2 and PS1 is blocked, and the excitation energy is released almost exclusively by fluorescence. In this case, the terminal fluorescence F_T is equal to the maximum fluorescence F_M. **(D)** Expanded section of (C) to determine the sudden fluorescence increase F_0 and the maximum fluorescence F_M. These values are used to quantify the quantum yield (Φ_{maxPS2} = 0.7 for this particular example).

Excitation with 440 nm laser light as actinic source (exciting the soret band) was most efficient and guaranteed an almost exclusive fluorescence of PS2 chlorophyll a, as there was no fluorescence of PBS and almost none (approx. 2%) of PS1 in the emission spectrum (Fig. 1B). The soret band excitation also takes advantage of a large Stokes shift to separate the laser reflection/scattering from the chlorophyll a emission signal at 680 nm [17]. In addition, a bandpass filter (676/29 nm) was placed in front of the detector to ensure that only photons emitted by PS2 were detected since PS1 fluorescence occurs above 700 nm [20]. Under these conditions, we can assume that only the fluorescence emission of the core antenna complex of PS2 is detected [21]. As the only type of chlorophyll in *S. elongatus* [19] *is* chlorophyll a [22], the detected signal is dominated by chlorophyll a from PS2.

In the following, we will briefly explain the temporal evolution of a typical fluorescence signal (F_V) and introduce three important parameters: minimum fluorescence (F_0), maximum fluorescence intensity (F_M) and terminal fluorescence (F_T) [23]. Almost in-

Preprints (www.preprints.org) | NOT PEER-REVIEWED | Posted: 10 November 2022 doi:10.20944/preprints202211.0199.v1

stantly, within a few picoseconds after actinic light irradiation, the photosynthetic chlorophyll fluorescence reaches an initial level called minimum fluorescence F_0 (Fig. 1D). Since the transfer of the photon energy via dipole-dipole interaction is much faster than the electron transfer by a sequence of redox reactions, a kind of energy pile-up occurs at the transition from the physical to the chemical energy transfer. The absorbed energy initially leads to a fast increase of the fluorescence intensity to the level F_M. F_0 is thereby the maximum energy that can be emitted without an electron backlog. If the photosystem is irradiated with an intensity too low to induce photochemistry, F_0 remains constant after the abrupt increase to the F_0-level, hence F_0 is independent of photochemical processes [24]. To reliably determine the maximal F_0 value, all PS2 reaction centers must be open and the corresponding electron acceptor (i.e. first stable acceptor, plastoquinone, Q_A) oxidized. This state can be achieved by 15 min dark adaptation of cyanobacterial cells [24]. If the dark adaptation time is longer or shorter, the result will be influenced by non-photochemical fluorescence quenching effects [24]. If dark adaptation is not fully achieved, F_0 increases and distorts the ratio of F_0 to the maximum fluorescence (F_M). After the abrupt rise to F_0, the variable fluorescence F_V rises to a maximum fluorescence F_M, since there is a temporal delay between the first absorption of a photon after dark adaptation and the start of the carbon reduction cycle. During the rise from F_0 to F_M, the electron acceptor Q_A becomes increasingly reduced [25] and an electron backlog occurs because reduced quinone (QH_2) cannot be re-oxidized fast enough and excess energy is released via fluorescence. Therefore, F_V reflects the redox state of Q_A [24]. F_M is only achieved when the actinic light intensity completely saturates all photosystems. In this case, all PS2 reaction centers are assumed to be in a closed state and all associated Q_A are completely reduced. If the actinic light is not saturating, the peak intensity does not reflect the maximum possible fluorescence of the system. Here, it is important to ensure that F_M is reached after a few milliseconds. To prevent the delay of F_M, the experiments were carried out in presence of 3-(3,4-Dichlorophenyl)-1,1-dimethylurea (DCMU). DCMU blocks the plastoquinone binding site (Q_B) and thereby prevents electron transport from Q_A to Q_B [26]. Consequently, all Q_A sites become completely reduced after onset of actinic light. This procedure enables to determine the true F_M value, since the energy absorbed by PS2 is completely emitted radiatively due to blocking of further electron transport. It must also be noted that high light intensities can also falsify F_M, because the photosystem is energetically overloaded and protective mechanisms are initiated that can delay F_M [27]. Thus, F_M is reached after a few seconds, until the cyanobacterium can react to the high light intensities and increases the energy dissipation by fluorescence. In the absence of DCMU, F_V decreases again as soon as Q_A becomes re-oxidized due to electron transport towards $NADPH/H^+$, essentially driven by PS1 activity. After a few minutes it reaches the steady state level F_T, illustrated in Fig. 1A [24]. This decrease is not possible in the presence of DCMU and F_M remains constant. In this case, F_M and F_T are technically the same (Fig. 1C) [26].

The analysis of the FFK enables us to obtain precise information about the intactness and efficiency of PS2 [28]. A good approximation for the current photochemical efficiency can be calculated by using F_0 and F_M:

$$\Phi_{maxPS2} = \frac{F_M - F_0}{F_M} = \frac{F_V}{F_M} \quad (1)$$

The current photochemical efficiency or quantum yield of PS2 Φ_{maxPS2} is a measure of the efficiency with which the excitation energy from the internal antenna pigments is adopted by the open P680 reaction centers [28]. Experiments that have determined the amount of oxygen produced as a function of light intensity show that Φ_{maxPS2} reflects, to a good approximation, the maximum relative electron transport efficiency [29]. In most plant species, Φ_{maxPS2} of about 0.83 can be expected [24]. However, determining the Φ_{maxPS2} of PS2 in cyanobacteria is not as straightforward as in plants, since additional antenna proteins, such as PBS, interfere with the measurement, distort the result and are the main reason for lower Φ_{maxPS2} yields [30]. After careful elimination of all interfering factors de-

 doi:10.20944/preprints202211.0199.v1

scribed above (DCMU application, narrow-band 440 nm laser excitation, use of a band-pass filter), the value for Φ_{maxPS2} of around 0.8 can also be expected for *S. elongatus* [30] [31].

The major challenge of the current work is to detect the fluorescence signal of a single cyanobacterium which is embedded in an optical microcavity. For this reason, the microcavity with embedded cyanobacteria is mounted on the scanning stage of a confocal microscope and one bacterium is centered in the focal volume of the high numerical aperture (NA) objective lens. The large NA ensures that a large fraction of the photons emitted by the excited bacterium can be collected. At a laser power of 2 nW, a single bacterial cell emitted statistically only 60 photons per millisecond at the fluorescence maximum (F_M) measured after the objective lens but before the cover slip on which the cyanobacteria are placed. Only about half the bacterium is illuminated by the diffraction limited excitation spot. In addition, to resolve the sudden fluorescence increase F_0 in the time domain, highly sensitive and fast-responding detectors must be used (rise time < 2 ns; for more details see Material and Methods). Due to low photon emission rate (compare Fig. 1D), a computer assisted evaluation is necessary to carry out the data analysis. To determine the fast increase in the F_0 emission, the raw data set was, therefore, smoothed by a Gaussian filter (Fig. 1D, blue line). The maximum of the first and second derivatives of the smoothed data set indicates F_0, since it is located in between these two extrema. The fluorescence maximum F_M was obtained by averaging all values in a temporal window ranging from 0.08 s to 1.00 s after F_0 (Fig. 1D, red dashed line indicates start of temporal window).

2.2 Measurement results

The quantum yield of individual cyanobacteria was measured and analyzed via their fluorescence response. For this purpose, the 440 nm laser (continuous wave mode) was precisely focused on one bacterium. The cross-section of a bacterium was approximated by a 1x2 μm ellipse.

Preprints (www.preprints.org) | NOT PEER-REVIEWED | Posted: 10 November 2022 doi:10.20944/preprints202211.0199.v1

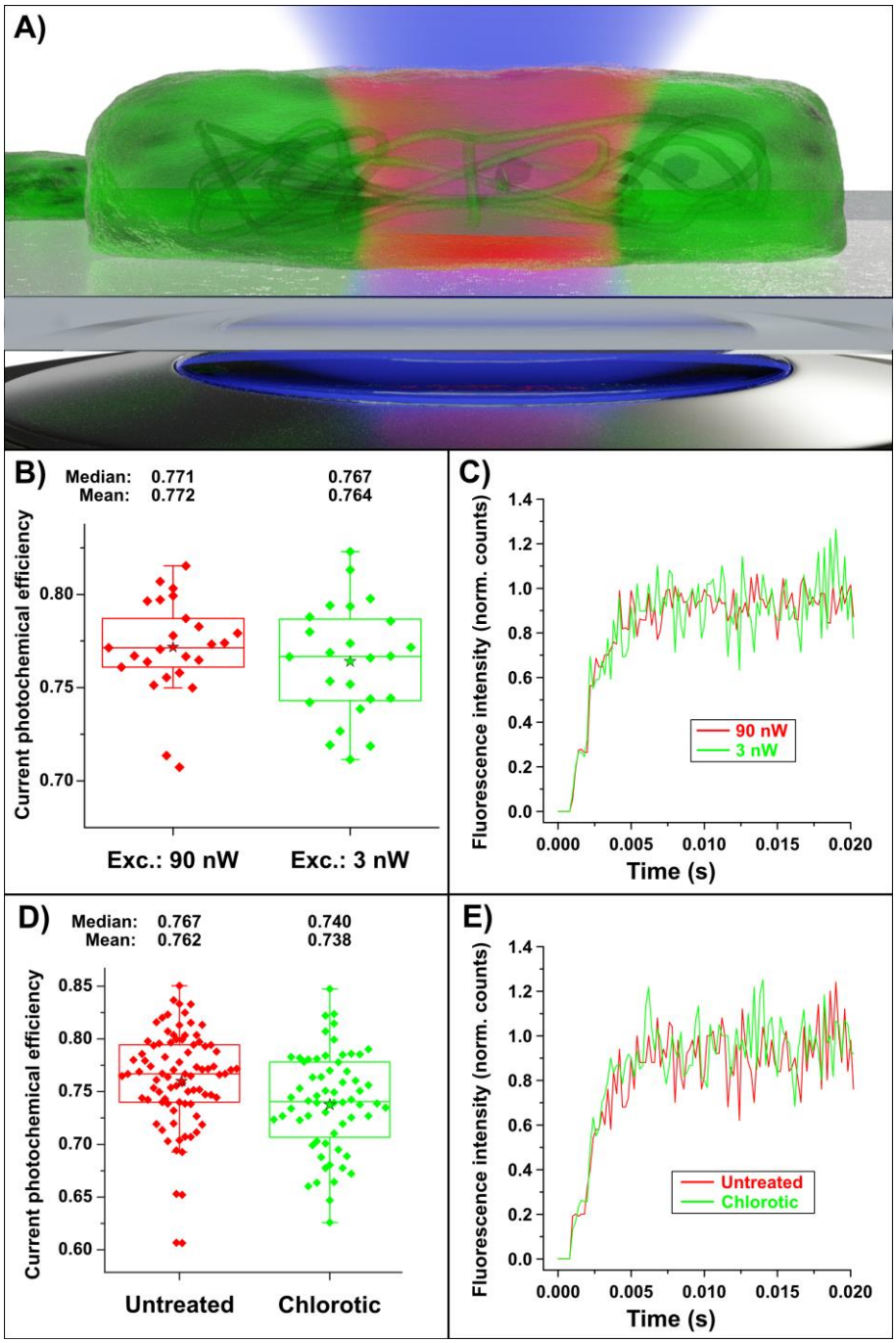

Figure 2. (A) Schematic illustration of a single bacterium on a glass coverslip in the focal volume of a high numerical aperture (NA = 1.4) objective lens. **(B)** Boxplot of the quantum yield of *S. elongatus* irradiated by 90 nW (red dots) and 3 nW (green dots) laser power to prove the independence of the photosynthetic efficiency from the laser power. There is no significant difference between 90 and 2 nW (two-tailed t-test, $p = 0.343$). **(C)** Two representative fluorescence curves recorded with a laser excitation intensity of 90 nW (red curve) and 3 nW (green curve). The curves were normalized to F_M because different amounts of chlorophyll are measured due to different bacteria sizes allowing a direct comparison. **(D)** Boxplot of the effective quantum yield of *S. elongatus* in free-space (red curve) and chlorotic cells (nitrogen starved) in free-space (green curve). Statistically, the median of the quantum yields of the free-space and the chlorotic bacteria differ significantly (two-tailed t-test $p = 3.10 \cdot 10^{-3}$). **(E)** Two representative fluorescence curves (normalized to F_M) of untreated cyanobacteria (red curve) and cyanobacteria grown under chlorotic conditions (green curve).

As a guide for the optimal light intensity for the following experiments we used the standard setting of commercial chlorophyll fluorescence curve analysis devices of approx. 3000 µmol photons · s-1 · m-2 [24], which is equivalent to a 440 nm laser power of 1.28 nW

Preprints (www.preprints.org) | NOT PEER-REVIEWED | Posted: 10 November 2022 doi:10.20944/preprints202211.0199.v1

per bacterium. To test for any effect in variations of irradiation intensity on the quantum yield, FFK curves of different individual bacteria from the same growth culture were measured with different laser intensities (see Fig. 2B/C).

As shown in Fig. 2B, the quantum yield of individual bacteria is the same for a laser exposure of 90 nW and 3 nW, as the difference of their median lies within the two statistical distributions (two-tailed t-test, $p = 0.343$). This indicates that the difference of the quantum yield cannot be attributed to unequal irradiation conditions. Under these conditions, a change in the quantum yield could therefore only be caused by the nature of the surrounding optical field. In order to test the lower limitation of the FFK in a single cell, the quantum yield of chlorotic cyanobacteria was recorded. The chlorosis of the cyanobacteria was induced by nitrogen starvation, which induces the degradation of photosynthetic pigments, in particular those of the PCBs, whilst the bulk of the photosystems stays intact [32]. As shown in Fig. 2D/E, the quantum yield in chlorotic cyanobacteria was significantly lower ($\Phi_{maxPS2} = 0.74$), compared to the yield from non-chlorotic cells ($\Phi_{maxPS2} = 0.77$).

An advantage of the single bacteria experiment over the classical population approach is that also the distribution of the quantum yields can be analyzed statistically and individually. The possibility to determine the quantum yield of a single bacteria allows to investigate extreme examples (outliers) in more detail. In a population experiment, small-scale differences of individual cells would be averaged.

An example, where a single bacteria approach is advantageous for FFK analysis, is when the photosynthetic light conditions vary on a small spatial scale, which is the case in an optical Fabry-Pérot microcavity. Here, each cyanobacterium experiences a different optical field. Fabry-Pérot microcavities consist of two semitransparent mirrors (quality factor, $Q = 98$) with an optical path length allowing resonances in the visible spectral range. For analysis in the microcavity, the cyanobacteria were embedded in a BG-11 agarose matrix to restrict spatial drift [9]. In the set-up, the cyanobacteria located in the microcavity were irradiated with 440 nm laser light from below and the residual fluorescence recorded through a high-NA objective lens ($NA = 1.4$) (see Fig. 3A). More details about the experimental setup were published before [9] and also given in the Materials and Methods.

Preprints (www.preprints.org) | NOT PEER-REVIEWED | Posted: 10 November 2022 doi:10.20944/preprints202211.0199.v1

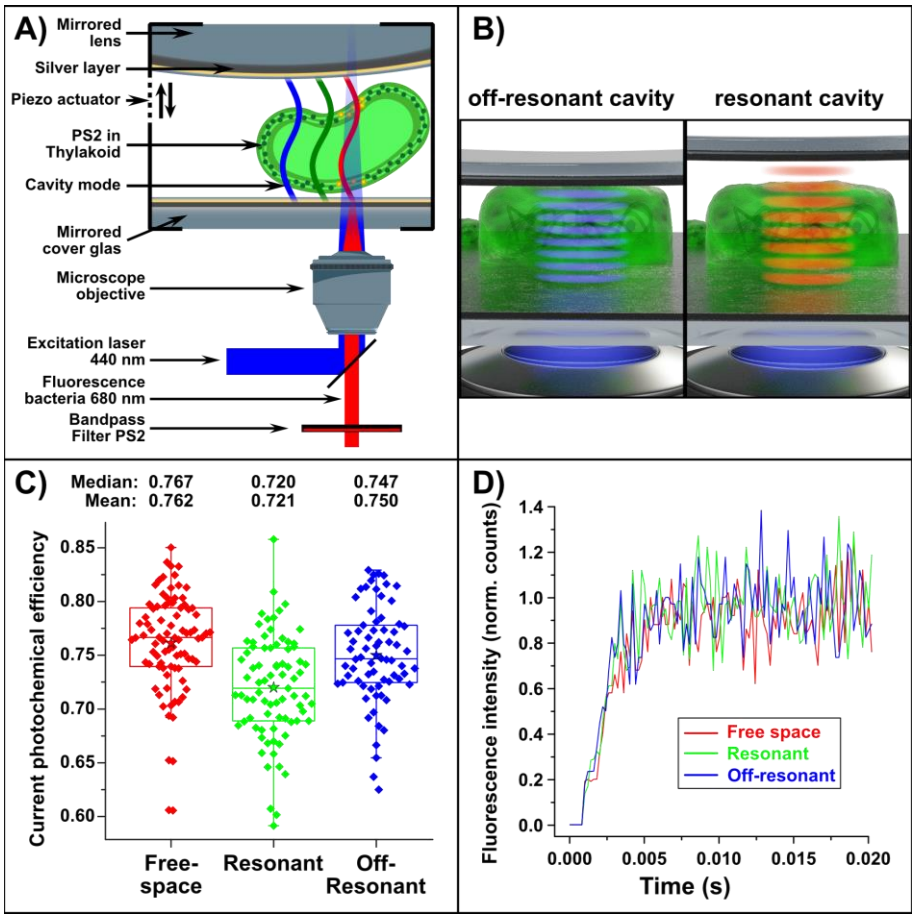

Figure 3. (A) Layout of the experimental set-up. A laser (440 nm, continuous wave) is focused by an objective lens onto a single bacterium in the microcavity that consists of two semi-transparent silver mirrors. The fluorescent light of the bacterium is transmitted by the beam splitter and directed to a detector. **(B)** Illustration of *S. elongatus* in a microcavity (consisting of two very close silver mirrors). On the right, bacterial fluorescence is resonant with the microcavity mode (red waves), which leads to strong coupling and splitting of the energy levels [9]. On the left, *S. elongatus* is illustrated in an off-resonant microcavity. **(C)** Boxplot of the quantum yield of *S. elongatus* in free-space (red dots), in a resonant (green dots) and an off-resonant (blue dots) microcavity. The quantum yield drops significantly inside the resonant microcavity (two-tailed t-test: compared to free-space: $p = 7.54 \cdot 10^{-8}$; compared to off-resonant microcavity: $p = 1.52 \cdot 10^{-4}$), with otherwise equal ambient conditions in both series of measurements. Statistically, the free-space and off-resonant measurement series do not differ (two-tailed t-test, $p = 0.12$). **(D)** Three representative fluorescence curves (normalized to F_M) of cyanobacteria in free-space (red curve), in a resonant microcavity (green curve) and an off-resonant cavity (blue curve).

In the first series, the FFK measurements were performed in free-space (see Fig. 3C/D, red color). The second series is recorded in a microcavity resonant to the absorption/emission at 680 nm (see Fig. 3C/D, green and illustration in Fig. 3B, right) and in the third series in an off-resonant microcavity (see Fig. 3C/D, blue and illustration in Fig. 3B, left) with a resonance set at approx. 500 nm. The largest quantum yield was observed in free-space and in the off-resonant microcavity. In contrast, there is a significant difference between the quantum yield in the off-resonance and the on-resonance ($p = 1.52 \cdot 10^{-4}$) microcavity, as well as between free-space and the resonant ($p = 7.54 \cdot 10^{-8}$) microcavity (Fig. 3C). Detailed values of the absolute, F_0-normalized and F_M-normalized data of quantum yield measurements in free-space, resonant and off-resonant microcavity are given in the supplementary information Table S1. Hence, only the resonant microcavity had a significant reductive impact on the quantum yield of single cyanobacteria, which also corresponds to previous fluorescence lifetime measurements of microcavity-enclosed

Preprints (www.preprints.org) | NOT PEER-REVIEWED | Posted: 10 November 2022 doi:10.20944/preprints202211.0199.v1

cyanobacteria [9]. Since the same ambient conditions prevail in the free-space and resonant microcavity, we can assume that the quantum yield is solely influenced by the special light conditions, i.e. the coherence of the optical field inside the resonant microcavity.

3. Discussion

We have developed a method to reliably determine the quantum yield of individual living cyanobacteria and demonstrated the reliability of the method. Moreover, we show that the measurements tolerate slight variations in the excitation intensity of the actinic light. To our opinion, the approach applied here and in our previous publication [9] are the first examples that an optical cavity enables the interrogation of biological systems in terms of quantum physical phenomena, theoretically proposed recently [33].

An especially interesting scenario is observed when the microcavity resonance coincides with the fluorescence and absorption maximum of the cyanobacterium (see Fig. 1B), where the excitation energy can coherently oscillate back and forth between the electromagnetic field in the microcavity and the photosynthetic pigments. This leads to so called strong light-matter coupling resulting in a polaritonic state, which manifests itself as a double-peaked microcavity transmission spectrum with a peak spacing called vacuum Rabi splitting [10].

The spread in the single cell experimental data most likely originates from the biological variation in the photosynthesis quantum yield of individual whole cyanobacteria. Impressively, our method can be used to show such differences. The magnitude of the spread might also allow deriving inferences about other biological effects, such as non-obvious deficiency symptoms or suboptimal environmental conditions of a bacterial culture. Our highly spatially resolved and direct measurements also demonstrate that cyanobacteria execute photosynthesis to different extents in the optical microcavity. Since the quantum yields differ significantly between a resonant and an off-resonant microcavity, it is reasonable to propose that the coherent optical field in the microcavity has a significant effect on the energy transfer in PS2 *in vivo*.

Our method allows us to study the microcavity influences on a single cyanobacterium. We are of the opinion that such a method will be helpful for future researchers to unravel remaining open questions of photosynthesis, e.g., about the efficiency of optical to chemical energy conversion.

4. Materials and Methods

4.1 Experimental set-up

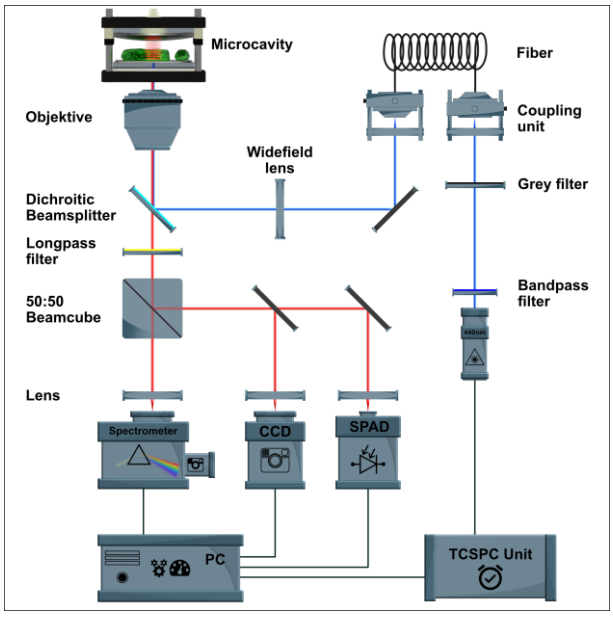

Figure 4. Used home-built semi confocal microscope.

Preprints (www.preprints.org) | NOT PEER-REVIEWED | Posted: 10 November 2022 doi:10.20944/preprints202211.0199.v1

A home-built confocal scanning microscope was used for the measurements in this work. The excitation light source is a laser diode (LDH-D-C-440, PicoQuant GmbH, Germany) operated in continuous wave mode with an excitation wavelength of 440 nm. The beam is directed *via* two mirrors through a clean-up interference filter (MaxDiode™ LD01-439/8-12.5, Semrock Inc., USA) onto a lens, which couples the beam into a single-mode glass fiber (P1-405 BPM-FC-2, Thorlabs Inc., USA). After the decoupling unit, the excitation light is passed through various gray filters and then onto a swiveling lens. This lens can be used to focus on the back aperture of the objective lens to acquire widefield images. After the lens, the beam is reflected by a dichroic beam splitter, which is positioned at a 45° angle to the propagation direction (F48-487 Laser Beam Splitter zt 488, AHF Analysentechnik AG, Germany). The beam splitter reflects light with wavelengths below 488 nm, whereas it transmits light with longer wavelengths. The reflected beam is now focused on the sample through an oil objective lens (Zeiss Plan-Apochromat, 100x, 1.4 Oil DIC, Carl Zeiss AG, Germany). Micrometer screws are used for coarse positioning of the sample and a piezo-controlled scanning stage (P-733.3CD, Physik Instrumente (PI) GmbH & Co. KG, Germany) allows sample scanning in three spatial dimensions. The fluorescence light emitted by the sample is collected by the same objective lens and transmitted through a beam splitter. An additional long-pass filter (488 LP Edge Basic long-pass filter, BLP01-488R-25, Semrock Inc., USA) and a band-pass filter (BrightLine® FF01-676/29-25, Semrock Inc., USA) are used to filter the detected signal. Confocal images of the fluorescence intensity are acquired by a single photon avalanche diode (SPAD) (PDM Series, Micro Photon Devices, Italy). The SPAD is coupled with a TCSPC unit (HydraHarp 400, PicoQuant GmbH, Germany) for the acquisition of time-correlated fluorescence traces. Spectra are acquired with a spectrometer (Acton SP300i, Princeton Instruments, USA) with a thermoelectrically cooled CCD camera (PIXIS 100, Princeton Instruments, USA). With widefield illumination, videos or images can be recorded in real time. The scanning stage, the SPAD, the laser diode and the TCSPC unit are controlled by the SymphoTime® software (PicoQuant GmbH, Germany). Fluorescence spectra are acquired with the software Winspec® (Princeton Instruments, USA). This software controls the monochromator and the corresponding CCD camera.

4.2 Preparation of microcavity mirrors

The mirror preparation was achieved by evaporating a 3 nm chromium layer on a glass cover slip to ensure that the following layers adhere well. Next, the reflective silver layer with a thickness of 30 nm or 60 nm for the lower and upper mirror, respectively, was vapor-deposited. A gold layer (5 nm) and an SiO_2 layer (20 nm) serves as a coating layer, since silver is very susceptible to oxidation and damage and is bactericidal [34]. The structure of these layers creates a microcavity with a quality factor of Q = 98. The distance between the two mirrors is adjusted very precisely by a piezo actuator. The custom-built holder is mounted on a stage scanning confocal microscope to measure the fluorescence of single cyanobacteria.

4.3 Light intensity measurements

The light intensity for the cultivation for *S. elongatus* was measured with a Li-Cor Li-189 radiometer from Heinz Walz GmbH (Germany). The laser power was measured with an Optical Power Meter Model 1830-C and a Sensor Model 818-SL, both from Newport Corporation (USA).

4.4 Bacterial cultivation conditions

Synechococcus elongatus PCC 7492 was cultivated under photoautotrophic conditions under continuous light with an intensity of around 30 µmol photons · s^{-1} · m^{-2} (Lumilux de Lux, Daylight, Osram). The cultivation was performed in 50 mL BG11 medium [19] supplemented with 5 mM $NaHCO_3$ in 100 mL Erlenmeyer flasks at 28 °C and continuous shaking (120-130 rpm).

Nitrogen-starved, chlorotic cells were obtained as previously described [35] with slight modifications. Exponentially grown *S. elongatus* cells in BG11 were harvested by centrifugation at room temperature (3.500 x*g*, 10 min), the supernatant was discarded, and

the cell pellet was washed twice with 50 mL $NaNO_3$-free BG11-medium (BG11-0). After that the cultures were cultivated in BG11-0 at light intensities of 50-60 µmol photons · s^{-1} · m^{-2} for 1 day.

4.5 Bacteria preparation

The cyanobacteria were treated with a 10 µmol 3-(3,4-Dichlorophenyl)-1,1-dimethylurea (DCMU) solution. 20 µL of a *S. elongatus* suspension were embedded in a low-melting agarose matrix (prepared with BG11 [19] medium) to prevent cell movement.

Supplementary Materials: The following supporting information can be downloaded at: www.mdpi.com/xxx/s1, They contain additional information, additional measurements, a comparison of absolute measurement data, the influence of a pulsed laser on the photosystem, Figure S1-S2; Table S1.

Author Contributions: T.R. and J.R. performed the experiments and analyzed the data with input from K.F., K.H., A.J.M. and S.z.O.-K. T.R. and F.W. wrote the manuscript with proofreading input from K.F., K.H., A.J.M., S.z.O.-K. and J.R.

Funding: A.J.M., F.W. and K.H. acknowledge support by the VW foundation (project title: A quantum beat for life) and the Deutsche Forschungsgemeinschaft (ME 1600/13-3; HA 2146/23-1; SFB 1101/D02 and Z02).

Data Availability Statement: Data are available in the main text or the supplementary materials. Further material is available from the corresponding author upon request.

Acknowledgments: The authors would like to thank the native speaker Dr. Kenneth Berendzen for English proofreading of the manuscript.

Conflicts of Interest: The authors declare no conflict of interest.

References

1. Schirrmeister, B.E.; de Vos, J.M.; Antonelli, A.; Bagheri, H.C. Evolution of Multicellularity Coincided with Increased Diversification of Cyanobacteria and the Great Oxidation Event. *Proc. Natl. Acad. Sci.* **2013**, *110*, 1791–1796, doi:10.1073/pnas.1209927110.
2. Holland, H.D. The Oxygenation of the Atmosphere and Oceans. *Philos. Trans. R. Soc. B Biol. Sci.* **2006**, *361*, 903–915, doi:10.1098/rstb.2006.1838.
3. Keeling, P.J. The Number, Speed, and Impact of Plastid Endosymbioses in Eukaryotic Evolution. *Annu. Rev. Plant Biol.* **2013**, *64*, 583–607, doi:10.1146/annurev-arplant-050312-120144.
4. Mančal, T. A Decade with Quantum Coherence: How Our Past Became Classical and the Future Turned Quantum. *Chem. Phys.* **2020**, *532*, 110663, doi:10.1016/j.chemphys.2019.110663.
5. Maxwell, K.; Johnson, G.N. Chlorophyll Fluorescence—a Practical Guide. 10.
6. Küpper, H.; Benedikty, Z.; Morina, F.; Andresen, E.; Mishra, A.; Trtílek, M. Analysis of OJIP Chlorophyll Fluorescence Kinetics and Q A Reoxidation Kinetics by Direct Fast Imaging. *Plant Physiol.* **2019**, *179*, 369–381, doi:10.1104/pp.18.00953.
7. Kautsky, H.; Hirsch, A. Neue Versuche zur Kohlens$\diamond$ureassimilation. *Naturwissenschaften* **1931**, *19*, 964–964, doi:10.1007/BF01516164.
8. Simis, S.G.H.; Huot, Y.; Babin, M.; Seppälä, J.; Metsamaa, L. Optimization of Variable Fluorescence Measurements of Phytoplankton Communities with Cyanobacteria. *Photosynth. Res.* **2012**, *112*, 13–30, doi:10.1007/s11120-012-9729-6.
9. Rammler, T.; Wackenhut, F.; zur Oven-Krockhaus, S.; Rapp, J.; Forchhammer, K.; Harter, K.; Meixner, A.J. Strong Coupling between an Optical Microcavity and Photosystems in Single Living Cyanobacteria. *J. Biophotonics* **2021**, doi:10.1002/jbio.202100136.
10. Boca, A.; Miller, R.; Birnbaum, K.M.; Boozer, A.D.; McKeever, J.; Kimble, H.J. Observation of the Vacuum Rabi Spectrum for One Trapped Atom. *Phys. Rev. Lett.* **2004**, *93*, 233603, doi:10.1103/PhysRevLett.93.233603.
11. Purcell, E.M. Spontaneous Emission Probabilities at Radio Frequencies. In *Confined Electrons and Photons: New Physics and Applications*; Burstein, E., Weisbuch, C., Eds.; Springer US: Boston, MA, 1995; pp. 839–839 ISBN 978-1-4615-1963-8.
12. Chizhik, A.I.; Chizhik, A.M.; Khoptyar, D.; Bär, S.; Meixner, A.J.; Enderlein, J. Probing the Radiative Transition of Single Molecules with a Tunable Microresonator. *Nano Lett.* **2011**, *11*, 1700–1703, doi:10.1021/nl200215v.
13. Casella, S.; Huang, F.; Mason, D.; Zhao, G.-Y.; Johnson, G.N.; Mullineaux, C.W.; Liu, L.-N. Dissecting the Native Architecture and Dynamics of Cyanobacterial Photosynthetic Machinery. *Mol. Plant* **2017**, *10*, 1434–1448, doi:10.1016/j.molp.2017.09.019.
14. Rexroth, S.; Nowaczyk, M.M.; Rögner, M. Cyanobacterial Photosynthesis: The Light Reactions. In *Modern Topics in the Phototrophic Prokaryotes: Metabolism, Bioenergetics, and Omics*; Hallenbeck, P.C., Ed.; Springer International Publishing: Cham, 2017; pp. 163–191 ISBN 978-3-319-51365-2.

15. Kondou, Y.; Nakazawa, M.; Higashi, S.; Watanabe, M.; Manabe, K. Equal-Quantum Action Spectra Indicate Fluence-Rate-Selective Action of Multiple Photoreceptors for Photomovement of the Thermophilic Cyanobacterium Synechococcus Elongatus¶. *Photochem. Photobiol.* **2007**, *73*, 90–95, doi:10.1562/0031-8655(2001)0730090EQASIF2.0.CO2.
16. Kennis, J.T.M.; Gobets, B.; van Stokkum, I.H.M.; Dekker, J.P.; van Grondelle, R.; Fleming, G.R. Light Harvesting by Chlorophylls and Carotenoids in the Photosystem I Core Complex of *Synechococcus Elongatus* : A Fluorescence Upconversion Study. *J. Phys. Chem. B* **2001**, *105*, 4485–4494, doi:10.1021/jp010382a.
17. Lahmi, R.; Sendersky, E.; Perelman, A.; Hagemann, M.; Forchhammer, K.; Schwarz, R. Alanine Dehydrogenase Activity Is Required for Adequate Progression of Phycobilisome Degradation during Nitrogen Starvation in Synechococcus Elongatus PCC 7942. *J. Bacteriol.* **2006**, *188*, 5258–5265, doi:10.1128/JB.00209-06.
18. Damjanović, A.; Vaswani, H.M.; Fromme, P.; Fleming, G.R. Chlorophyll Excitations in Photosystem I of *Synechococcus Elongatus*. *J. Phys. Chem. B* **2002**, *106*, 10251–10262, doi:10.1021/jp020963f.
19. Rippka, R.; Stanier, R.Y.; Deruelles, J.; Herdman, M.; Waterbury, J.B. Generic Assignments, Strain Histories and Properties of Pure Cultures of Cyanobacteria. *Microbiology* **1979**, *111*, 1–61, doi:10.1099/00221287-111-1-1.
20. Pfündel, E.E.; Klughammer, C.; Meister, A.; Cerovic, Z.G. Deriving Fluorometer-Specific Values of Relative PSI Fluorescence Intensity from Quenching of F 0 Fluorescence in Leaves of Arabidopsis Thaliana and Zea Mays. *Photosynth. Res.* **2013**, *114*, 189–206, doi:10.1007/s11120-012-9788-8.
21. Krause, G.H.; Weis, E. Chlorophyll Fluorescence and Photosynthesis: The Basics. 37.
22. Zouni, A.; Witt, H.-T.; Kern, J.; Fromme, P.; Krauss, N.; Saenger, W.; Orth, P. Crystal Structure of Photosystem II from Synechococcus Elongatus at 3.8 Å Resolution. *Nature* **2001**, *409*, 739–743, doi:10.1038/35055589.
23. van Kooten, O.; Snel, J.F.H. The Use of Chlorophyll Fluorescence Nomenclature in Plant Stress Physiology. *Photosynth. Res.* **1990**, *25*, 147–150, doi:10.1007/BF00033156.
24. Matyssek, R.; Herppich, W.B. Experimentelle Pflanzenökologie: Chlorophyllfluoreszenzanalyse. In *Handbuch der Geodäsie*; Freeden, W., Rummel, R., Eds.; Springer Reference Naturwissenschaften; Springer Berlin Heidelberg: Berlin, Heidelberg, 2018; pp. 1–56 ISBN 978-3-662-46900-2.
25. *Chlorophyll a Fluorescence: A Signature of Photosynthesis*; Papageorgiou, G.C., Govindjee, Eds.; Advances in photosynthesis and respiration; Kluwer Academic: Dordrecht, 2004; ISBN 978-1-4020-3217-2.
26. Campbell, D.; Hurry, V.; Clarke, A.K.; Gustafsson, P.; Öquist, G. Chlorophyll Fluorescence Analysis of Cyanobacterial Photosynthesis and Acclimation. *Microbiol. Mol. Biol. Rev.* **1998**, *62*, 667–683, doi:10.1128/MMBR.62.3.667-683.1998.
27. Herppich, W.B.; Herppich, M.; Tuffers, A.; von WILLERT, D.J.; Midgley, G.F.; Veste, M. Photosynthetic Responses to CO2 Concentration and Photon Fluence Rates in the CAM-Cycling Plant Delosperma Tradescantioides (Mesembryanthemaceae). *New Phytol.* **1998**, *138*, 433–440, doi:10.1046/j.1469-8137.1998.00137.x.
28. Baker, N.R. A Possible Role for Photosystem II in Environmental Perturbations of Photosynthesis. *Physiol. Plant.* **1991**, *81*, 563–570, doi:10.1111/j.1399-3054.1991.tb05101.x.
29. Bjoerkman, O.; Demmig, B. Photon Yield of O2 Evolution and Chlorophyll Fluorescence Characteristics at 77 K among Vascular Plants of Diverse Origins. *Planta* **1987**, *170*, 489–504, doi:10.1007/BF00402983.
30. Ogawa, T.; Sonoike, K. Effects of Bleaching by Nitrogen Deficiency on the Quantum Yield of Photosystem II in *Synechocystis* Sp. PCC 6803 Revealed by Chl Fluorescence Measurements. *Plant Cell Physiol.* **2016**, *57*, 558–567, doi:10.1093/pcp/pcw010.
31. Santabarbara, S.; Villafiorita Monteleone, F.; Remelli, W.; Rizzo, F.; Menin, B.; Casazza, A.P. Comparative Excitation-emission Dependence of the F_V / F_M Ratio in Model Green Algae and Cyanobacterial Strains. *Physiol. Plant.* **2019**, *166*, 351–364, doi:10.1111/ppl.12931.
32. Görl, M.; Sauer, J.; Baier, T.; Forchhammer, K. Nitrogen-Starvation-Induced Chlorosis in Synechococcus PCC 7942: Adaptation to Long-Term Survival. *Microbiology* **1998**, *144*, 2449–2458, doi:10.1099/00221287-144-9-2449.
33. Caruso, F.; Saikin, S.K.; Solano, E.; Huelga, S.F.; Aspuru-Guzik, A.; Plenio, M.B. Probing Biological Light-Harvesting Phenomena by Optical Cavities. *Phys. Rev. B* **2012**, *85*, 125424, doi:10.1103/PhysRevB.85.125424.
34. Konrad, A.; Metzger, M.; Kern, A.M.; Brecht, M.; Meixner, A.J. Controlling the Dynamics of Förster Resonance Energy Transfer inside a Tunable Sub-Wavelength Fabry–Pérot-Resonator. *Nanoscale* **2015**, *7*, 10204–10209, doi:10.1039/C5NR02027A.
35. Klotz, A.; Georg, J.; Bučinská, L.; Watanabe, S.; Reimann, V.; Januszewski, W.; Sobotka, R.; Jendrossek, D.; Hess, W.R.; Forchhammer, K. Awakening of a Dormant Cyanobacterium from Nitrogen Chlorosis Reveals a Genetically Determined Program. *Curr. Biol.* **2016**, *26*, 2862–2872, doi:10.1016/j.cub.2016.08.054.
36. Chizhik, A.; Schleifenbaum, F.; Gutbrod, R.; Chizhik, A.; Khoptyar, D.; Meixner, A.J.; Enderlein, J. Tuning the Fluorescence Emission Spectra of a Single Molecule with a Variable Optical Subwavelength Metal Microcavity. Phys. Rev. Lett. **2009**, 102, doi:10.1103/PhysRevLett.102.073002.